ACS Photonics

Article

pubs.acs.org/journal/apchd5

Near-Unity Unselective Absorption in Sparse InP Nanowire Arrays

Katherine T. Fountaine,*[,†,‡,§] Wen-Hui Cheng,[‡,§] Colton R. Bukowsky,[‡] and Harry A. Atwater[‡,§]

[†]NGNext, Northrop Grumman Aerospace Systems, 1 Space Park Drive, Redondo Beach, California 90278, United States

[‡]Department of Applied Physics and Materials Science and [§]Joint Center for Artificial Photosynthesis, California Institute of Technology, 1200 East California Boulevard, Pasadena, California 91125, United States

Supporting Information

ABSTRACT: We experimentally demonstrate near-unity, unselective absorption, broadband, angle-insensitive, and polarization-independent absorption, in sparse InP nanowire arrays, embedded in flexible polymer sheets via geometric control of waveguide modes in two wire motifs: (i) arrays of tapered wires and (ii) arrays of nanowires with varying radii. Sparse arrays of these structures exhibit enhanced absorption due to strong coupling into the first order azimuthal waveguide modes of individual nanowires; wire radius thus controls the spectral region of the absorption enhancement. Whereas arrays of cylindrical wires with uniform radius exhibit narrowband absorption, arrays of tapered wires and arrays with multiple wire radii expand this spectral region and achieve broadband absorption enhancement. Herein, we present an economic, top-down lithographic/etch fabrication method that enables fabrication of multiple InP nanowire arrays from a single InP wafer with deliberate control of nanowire radius and taper. Using this method, we create sparse tapered and multiradii InP nanowire arrays and demonstrate optical absorption that is broadband (450−900 nm), angle-insensitive, and near-unity (>90%) in roughly 100 nm planar equivalence of InP. These highly absorbing sparse nanowire arrays represent a promising approach to flexible, high efficiency optoelectronic devices, such as photodetectors, solar cells, and photoelectrochemical devices.

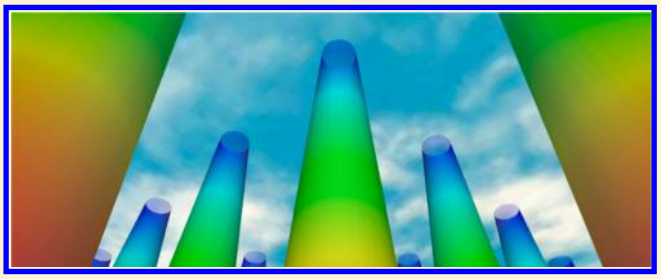

KEYWORDS: *nanowire, optoelectronic, waveguide, broadband absorber, photovoltaic*

Design of "perfect" absorbers and emitters is of considerable current interest and research in the nanophotonics and metamaterials fields.[1−3] Perfect absorbers and emitters can find applications in numerous fields across the electromagnetic spectrum, including light and thermal sources,[4−6] sensing,[7,8] and energy conversion.[5,9,10] Two types of near-unity or "perfect" absorption are straightforward to achieve: (1) a wavelength-sized resonator can be used for selective "perfect" absorption, absorption at a single frequency, polarization, and incidence angle,[11−14] and (2) an optically thick layer of lossy material can be used for unselective, "perfect" absorption, absorption over a large range of frequencies, angles, and polarizations.[15] However, many applications would benefit from a more comprehensive ability to tailor perfect absorber characteristics, such as achieving directional, spectrally broadband thermal emission of infrared radiation sources,[4,16] and broadband, angle-insensitive thin film perfect absorbers for high efficiency, lightweight photovoltaics.[15,17,18] To this end, recent work in the field has focused on the realization of selective perfect absorbers that are extremely thin,[1,13,19] actively tunable,[20,21] and wavelength, angle, or polarization-insensitive,[3,22,23] as well as unselective perfect absorbers with small form factors that are insensitive to angle, wavelength, or polarization.[9,10]

In this work, we focus on the design and fabrication of unselective perfect absorbers with small form factors using semiconductor nanowire arrays. Specifically, we examine sparse arrays of InP nanowires fabricated using a top-down lithographic pattern and etch procedure, followed by embedding in polydimethylsiloxane (PDMS) and mechanical removal from the substrate. These sparse arrays of vertically oriented, semiconductor nanowires represent a promising approach to flexible, lightweight, high efficiency, and low cost optoelectronic devices in sensing and energy applications, such as photodetectors,[24−26] bolometers,[27,28] solar cells,[10,29−31] and photoelectrochemical devices.[32,33] Currently in the photovoltaics field, the greatest challenge for use of III−V absorbers and cells is reducing cost/Watt.[34] Therefore, it is highly desirable to develop fabrication methods that reduce or eliminate costs associated with epitaxial growth and consumption of III−V compound semiconductor substrates. The wire array fabrication process described herein holds considerable promise for achieving these goals because many layers can be fabricated from a single compound semiconductor substrate. InP is of particular interest for wire array photovoltaics, and more broadly, InP has garnered much interest for nanowire-based optoelectronic devices due to its direct bandgap and low intrinsic surface recombination velocity,[35] which is critical to high performance in high surface area devices.

Received: May 16, 2016

DOI: 10.1021/acsphotonics.6b00341
ACS Photonics XXXX, XXX, XXX−XXX

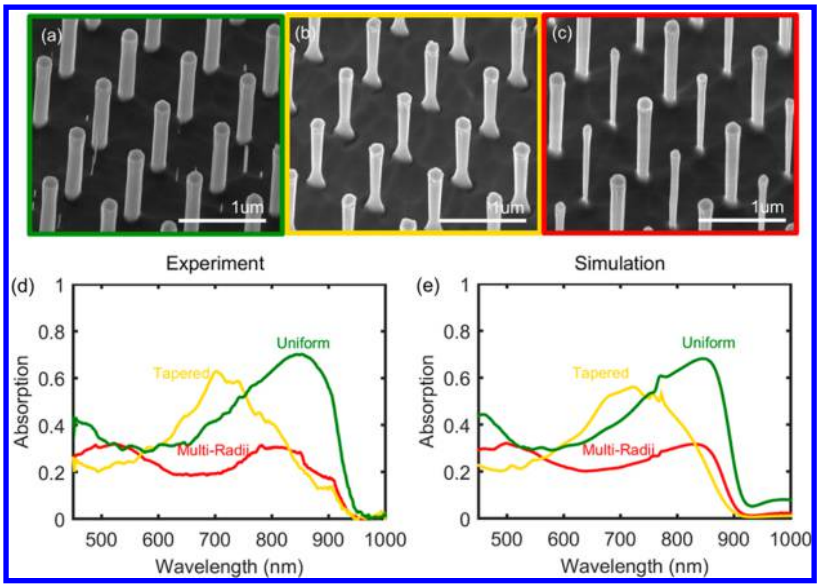

Figure 1. Comparison of uniform, tapered, and multiradii arrays. (a–c) Scanning electron micrographs of the uniform, tapered, and multiradii array, respectively, at a 30° tilt angle; (d) Absorption spectra for the PDMS-embedded arrays shown in (a–c), measured using an integrating sphere; (e) Simulated absorption spectra corresponding to the experimental results in (d), calculated using a weighted average of the range of nanowire geometries observed in the fabricated samples; see Table 1 of Supporting Information for array dimensions used in simulation. Colors are coordinated throughout the figure.

In recent years, the optical properties of semiconductor nanowire arrays have been the subject of great interest and intensive research.[36−39] Even at very low area fill fractions, semiconductor nanowire arrays exhibit strong optical absorption due to robust coupling into the waveguide modes of individual nanowires.[10,40] These arrays of essentially independent optical antennas have an optical response that is polarization-independent and angle-insensitive.[32] In a standard nanowire array with uniform wire radius, strong absorption is observed over a relatively narrow spectral region in which end-mediated coupling into guided modes is favorable.[32,41] Array geometry,[42−44] nanowire shape,[10,45−47] and order[48,49] have previously been shown both experimentally and theoretically to control the spectral position of this region by others. In previous work,[10] we theoretically studied different nanowire motifs within sparse arrays and, by optical design of the waveguide modes, predicted broadband absorption enhancements for specific nanowire array geometries and nanowire motifs, using constant material volume. Specifically, we optimized arrays with multiple nanowire radii and tapered nanowires and predicted >90% broadband absorption (Vis-NIR) in 150 nm planar equivalence. Herein, we develop a deliberate fabrication method for the desired nanowire array motifs and experimentally demonstrate broadband, polarization-independent, angle-insensitive, near-unity (>90%) absorption in sparse arrays of InP nanowires.

RESULTS AND DISCUSSION

In this section, we begin with a brief discussion of InP nanowire array design. Next, we validate our experimental and theoretical methods via a uniform InP nanowire array. Subsequently, we prove that nanowire taper induces peak broadening and multiple wire radii generate multiple peaks via characterization of very sparse InP nanowire arrays. Finally, we demonstrate near-unity broadband absorption in sparse arrays of tapered and multiradii InP nanowire arrays. Details on fabrication methods for precise control of nanowire motif and array geometry can be found in the Methods section.

Design of Nanowire Arrays. As previously stated, vertically oriented semiconductor nanowires act as cylindrical dielectric waveguides with high absorption loss. In sparse arrays, the nanowires are essentially noninteracting and, thus, their optical behavior is well-described by traditional waveguide theory.[50] The nanowires exhibit a primary absorption peak, which is due to end-mediated coupling into the HE_{11} waveguide mode. The HE_{11} mode is the TM-like, fundamental mode that has no cutoff and strong symmetry overlap with plane waves, facilitating strong in-coupling. In lossy nanowires, the spectral region of strong coupling and subsequent absorption enhancement occurs in the moderately guided portion of the HE_{11} modal dispersion.[40] The dominant role of the waveguide modes in the absorption enhancement translates to a strong correlation between nanowire radius and the spectral region of absorption enhancement and is used herein to guide the design of InP nanowire arrays. A radius range of 40 to 100 nm is needed to observe absorption enhancement in the visible up to the band edge of InP (450–925 nm).

Standard Nanowire Arrays. Initially, we examine a uniform nanowire array (r = 90 nm, h = 1.6 μm, a = 750 nm) to validate our theoretical framework as well as our experimental and simulation methods. This array, shown at a 30° tilt in Figure 2a, has a fill fraction of 4.4% and a planar equivalent thickness of ∼70 nm. Figure 2d displays the absorption spectrum (green line) for the array, after it was embedded in PDMS and peeled off of the substrate; the reflection spectra for the array in three different configurations, on substrate, embedded in PDMS, and on substrate, and embedded in PDMS and peeled off of the substrate, is contained in the Supporting Information. These experimental spectra give the expected results: we observe low reflectivity for the array in all cases and a primary absorption peak around 850 nm, corresponding to coupling into the HE_{11} waveguide mode. Figure 2e displays the corresponding simulated absorption

DOI: 10.1021/acsphotonics.6b00341
ACS Photonics XXXX, XXX, XXX−XXX

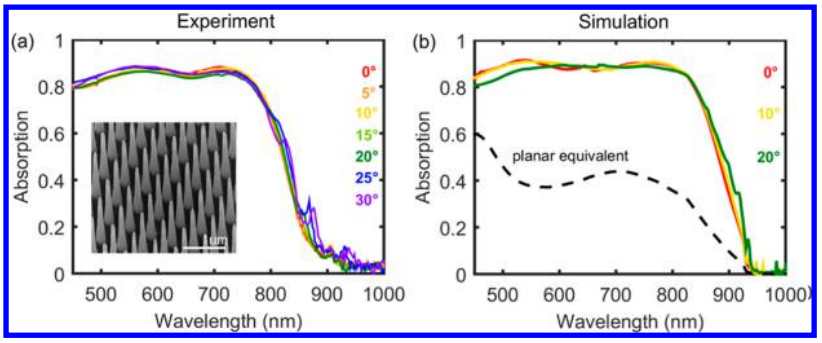

Figure 2. Characterization of tapered array. (a) Absorption spectra at various incident angles for the PDMS-embedded array (SEM image taken at a 30° tilt angle shown as inset), measured using an integrating sphere; (b) simulated spectra corresponding to the experimental results in (a) calculated using an average of three slight geometric variations representing the range of nanowire geometries observed in the fabricated sample; overlaid with the planar equivalent absorption spectra (108 nm thin film, black dashed); see Table 1 of Supporting Information for array dimensions used in simulation. Colors are coordinated throughout the figure.

spectrum (green line), which is a weighted average of spectra for nanowire array dimensions that capture the geometric variation observed in the fabricated sample (see Methods and Supporting Information for a detailed accounting of simulated array geometry). We found good agreement between experiment and simulation. Additional details on experimental and simulation methods can be found in the Methods section; the geometry of each simulated array can be found in the Supporting Information, along with a discussion of sources for deviation between simulated and experimental spectra.

Broadband Absorber Nanowire Arrays. The initial broadband absorber arrays presented herein were designed with the intention of demonstrating that tapered nanowires broaden the primary HE_{11} absorption peak and that multiple radii in a single array generate multiple absorption peaks. Therefore, sparse arrays of short nanowires were fabricated, and the multiradii subcell consisted of two different radii. Fabrication details can be found in the Methods section. The sparseness of these arrays and the use of only two distinct radii in the multiradii array resulted in more well-defined peak features compared with the slightly denser arrays of taller nanowires in the following section, which is particularly essential to the distinction of multiple peaks in the multiradii arrays that might otherwise blend into one extended peak due to experimental variation in the fabricated dimensions.

Figure 1a–c displays SEM images at 30° tilt of the sparse (a = 750 nm) uniform, tapered, and multiradii arrays, which have fill fractions (planar equivalent thicknesses) of 4.4% (70 nm), 2.3% (29 nm), and 2.3% (31 nm), respectively. The fill fractions and planar equivalent thicknesses were determined from image analysis, and the precise dimensions used in simulation can be found in the Supporting Information. Figure 1d,e displays the experimental and simulated absorption spectra for these arrays, demonstrating good qualitative agreement between simulation and experiment. Again, the simulated spectra were calculated using a weighted average of the range of nanowire geometries observed in the fabricated samples. The absorption spectrum of the tapered nanowire array (yellow) exhibits a broadened absorption peak in comparison to that of the uniform array (green) due to the spectral broadening of the HE_{11} waveguide mode that results from the continually varying radius from ∼55 to ∼75 nm; and the absorption spectrum of the multiradii nanowire array (red) exhibits two peaks, corresponding to the HE_{11} waveguide modes of the two different nanowire radii (r ∼ 40 and 80 nm). These results demonstrate that nanowire taper and multiple wire radii within a single array both extend the spectral range of absorption enhancement effected by nanowire array due optical engineering of the HE_{11} waveguide mode.

It is important to note that while the uniform array may appear to be outperforming the tapered and multiradii arrays in terms of integrated absorption, it is only because the uniform array contains more than twice the amount of InP. Additionally, the simulated spectra in Figure 1 employed broadband FDTD simulations with a polynomial fit to material data, which is imperfect near the band edge of InP and results in unphysical absorption beyond the band edge in the simulated spectra. A more thorough discussion of sources for deviation between simulated and experimental spectra can be found in the Supporting Information.

Near-Unity, Broadband Absorber Arrays. To achieve near-unity broadband absorption, slightly denser arrays of taller nanowires were fabricated for both the tapered nanowire and multiradii nanowire motifs. Additionally, the multiradii array consisted of a 4 wire subcell (2 × 2) to distribute the strong in-coupling region of the HE_{11} mode more evenly across the visible spectrum. Fabrication details can be found in the Methods section.

Figure 2 contains the results for an exemplary tapered nanowire array, with ∼1.6 μm tall nanowires with radii ranging from 30 to 110 nm, spaced 450 nm apart (SEM image taken at a 30° tilt in the inset of Figure 2a). The array has a fill fraction of 6.7% and contains 108 nm planar equivalence of InP; a detailed accounting of array dimensions can be found in the Supporting Information. The experimentally measured and simulated absorption spectra for the PDMS-embedded, tapered nanowire array are displayed in Figure 2a and b, respectively, as a function of incidence angle. The experimental data includes incidence angles from 0° to 30°, in 5° increments. The simulated data employed single wavelength FDTD simulations at 0°, 10°, and 20° and the spectra is a standard average of three slight geometric variations; the absorption of the planar equivalence (108 nm) is also overlaid for reference (black, dashed line). In all spectra, we find good qualitative agreement between simulation and experiment. A discussion of sources for quantitative deviation between simulated and experimental spectra can be found in the Supporting Information.

The tapered array demonstrates angle-insensitive broadband absorption, approaching 90% absorption across the visible. The PDMS front surface results in approximately a 5% broadband

DOI: 10.1021/acsphotonics.6b00341
ACS Photonics XXXX, XXX, XXX−XXX

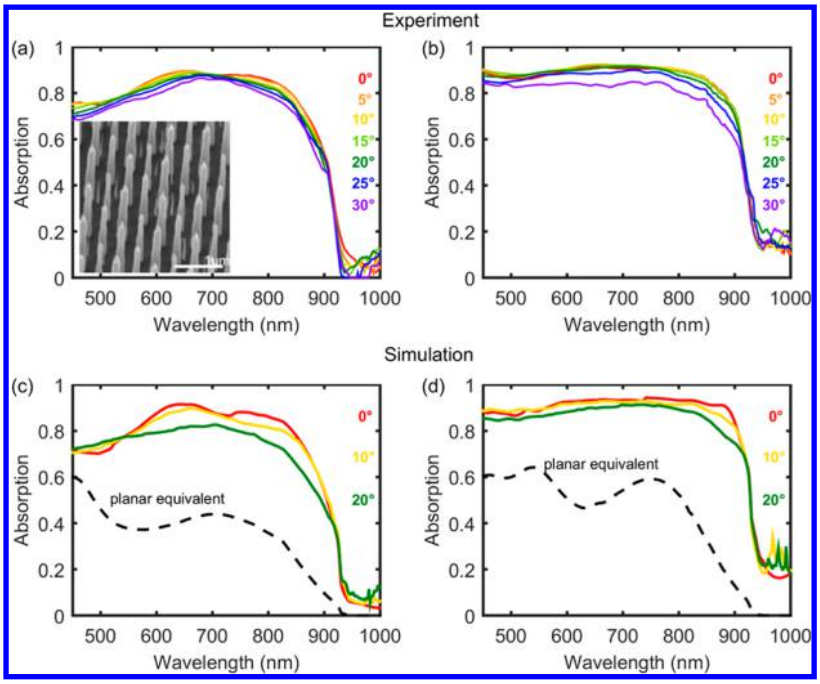

Figure 3. Characterization of multiradii array. (a, b) Absorption spectra at various incident angles for the PDMS-embedded array, (SEM image taken at a 30° tilt angle shown as inset of (a)), without and with a silver back reflector, respectively, measured using an integrating sphere; (c, d) simulated spectra corresponding to the experimental results in (a, b) calculated using a weighted average of three slight geometric variations representing the range of nanowire geometries observed in the fabricated samples, overlaid with the planar equivalent absorption spectra (104 and 208 nm thin films, black dashed); see Table 1 of Supporting Information for array dimensions used in simulation. Colors are coordinated throughout the figure.

reflectivity and the remainder is transmission losses due to incomplete absorption. Compared to the planar equivalent thin film of 108 nm (black, dashed line in Figure 2b), the nanowire array exhibits broadband absorption enhancements across the visible spectrum. These absorption enhancements occur due to strong coupling into the HE_{11} waveguide mode, which has been engineered to occur over a broad spectral region via wire taper. Absorption drops off beyond 800 nm because there is insufficient wire length at the larger wire radii to observe significant absorption enhancements. Additionally, the noise in both the experimental and simulated spectra is attributed to residual pieces of the Cr etch mask; contributions of the Cr mask to the array absorption were quantified via simulation and found to be negligible (see Supporting Information for details).

Figure 3 displays the results for an exemplary multiradii nanowire array, with ~1.75 μm tall nanowires with radii ranging from 35 to 115 nm, spaced 520 nm apart (SEM image at 30° tilt shown as the inset of Figure 3a). The array has a fill fraction of 6% and contains 104 nm planar equivalence of InP; a detailed accounting of array dimensions can be found in the Supporting Information. The experimentally measured and simulated absorption spectra for the PDMS-embedded, multiradii nanowire array are displayed in Figure 3a and c, respectively, as a function of incidence angle. To further push the array absorption toward near-unity, a silver back reflector was deposited to achieve two-pass absorption and the resulting experimental and simulated absorption spectra are shown in Figure 3b,d. The experimental data includes incidence angles from 0° to 30°, in 5° increments. The simulated data employed single wavelength FDTD simulations at 0°, 10°, and 20° and the spectra is a weighted average of three slight geometric variations; the absorption of the planar equivalence (104 nm for single pass, 208 nm for two-pass) is also overlaid for reference (black, dashed line). In all spectra, we find good qualitative agreement between simulation and experiment. A discussion of sources for quantitative deviation between simulated and experimental spectra can be found in the Supporting Information.

The multiradii array demonstrates angle-insensitive broadband absorption, approaching 90% absorption in a single pass and exceeding 90% with a silver back reflector up to the band edge of InP ($\lambda \sim 925$ nm). Again, the PDMS front surface results in approximately a 5% broadband reflectivity, which accounts for nearly all of the loss when the array has a back reflector. In the single pass case, the remainder is transmission losses due to incomplete absorption. Compared to the planar equivalent thin films (104 nm for single pass, 208 nm for double pass; black, dashed lines in Figure 3c,d), the nanowire array exhibits broadband absorption enhancements across the visible spectrum. These absorption enhancements occur due to strong coupling into the HE_{11} waveguide mode, which has been engineered to occur over a broad spectral region via multiple wire radii that span the appropriate radius range.

In the single pass case, absorption is slightly lower in the blue, exhibiting the inverse problem to the tapered array (absorption dropped off in the red); this discrepancy occurs for two reasons: (1) the radii range of the multiradii array is slightly larger than the tapered array, resulting in a red-shift of the absorption, and (2) the largest wire radius of the subcell targets the red region of the spectrum, which is more effective than the very edge of the wire taper.

In the double pass case, the absorption is nearly flat at >90% absorption, up to the band edge of InP, but does not drop to zero beyond the band edge. The absorption beyond the band edge occurs in the silver back reflector, due to the HE_{11} mode field enhancements at the interface. The silver absorption is only significant beyond the band edge of InP; up to the band edge, the vast majority of the absorption occurs in the InP.

DOI: 10.1021/acsphotonics.6b00341
ACS Photonics XXXX, XXX, XXX−XXX

Absorption in each material was quantified via simulation and can be found in the Supporting Information.

CONCLUSION

In this work, we experimentally demonstrated near-unity, unselective absorption, absorption that is broadband, polarization-independent, and angle-insensitive, in sparse arrays of InP nanowire arrays, enabled by controlled fabrication of nanowire motifs optimized via optical design. We explored two motifs, tapered nanowires and arrays of nanowires with varying radii, that aim to enhance absorption across a wide spectral range by optical design of the HE_{11} waveguide mode dispersion and developed deliberate fabrication methods for the realization of these designs. Initially, we demonstrated that wire taper broadens the HE_{11} mode absorption peak and that incorporation of multiple wire radii results in multiple HE_{11} mode absorption peaks. Subsequently, we designed and fabricated sparse InP nanowire arrays using both wire taper and multiple wire radii that achieved near-unity, unselective absorption. Specifically, we achieved greater than 90% absorption up to the band edge of InP in a multiradii nanowire array with a back reflector that contained approximately 100 nm planar equivalence of InP. These semiconductor-based, spectrally and angularly unselective absorbers have great potential for flexible, high efficiency, and low-cost optoelectronic devices in energy and sensing applications.

METHODS

Fabrication. InP nanowire arrays were fabricated top-down from InP wafers (2″ AXT, n-type, sulfur-doped, (100) orientation), using inductively coupled plasma reactive ion etching (ICP-RIE). Wafers were cleaned via sequential sonication for 10 min in water, IPA, acetone, and water. A piranha clean step was omitted because the existence of the native InP_xO_y facilitated adhesion of the hard mask layers.

Two different hard masks were used in this work: SiO_2 and Cr. The SiO_2 mask was approximately 400 nm thick and deposited via RF sputtering (SiO_2 target, 3 mTorr Ar atmosphere, 200 W forward power). The pattern was defined in the mask via a direct electron beam lithography write into negative tone, MaN-2403 resist, followed by a pseudo-Bosch RIE step (5 mTorr, 1000 W ICP forward power, 25 W RF forward power, 10 °C, 26 sccm SF_6, 35 sccm C_4F_8) to transfer the pattern from the resist into the SiO_2. For the Cr hard mask, the pattern was defined via a direct electron beam lithography write into a bilayer of positive tone resist (PMMA495-A4/PMMA95-A4), followed by electron beam deposition of a 50 nm Cr layer (0.5 $A{\cdot}s^{-1}$, 10^{-6} Torr) and lift-off of the resist. The Cr mask was preferable for deep InP etches because it exhibited a much higher etch selectivity (~40:1) than the SiO_2 mask (~4:1). The higher selectivity of the Cr mask also provided increased control over the axial profile of the nanowire because lateral etching of the Cr mask was consequently less significant.

A $Cl_2/H_2/CH_4$ etch (4 mTorr, 2200 W ICP forward power, 200 W RF forward power, 28 sccm H_2, 32 sccm Cl_2) was used to transfer the pattern into the InP for the realization of nanowire arrays. The table temperature was set to 60 °C and no thermal contact between the sample and the carrier wafer was omitted to achieve etch temperatures of ~300 °C to ensure sufficient volatility of the In etch products. Because CH_4 provides sidewall passivation, its flow was varied between 24 and 30 sccm to control the degree of sidewall taper from normal taper to inverse taper, respectively. For the arrays discussed herein, normal taper, no taper, and inverse taper were obtained at 24, 26, and 30 sccm, respectively.

To exfoliate the nanowire arrays from the InP substrate, the samples were covered with a thick layer of 10:1 PDMS solution, degassed for 20 min, baked overnight at 80 °C, and mechanically peeled-off the substrate after cooling. All SEM images were taken on wafer, prior to embedding in PDMS.

Optical Characterization. All experimental optical spectra were obtained using a Fianium laser as a tunable source and a home-built integrating sphere setup with silicon photodiode detectors.[51] Reflection and transmission (when relevant) spectra are composed of 276 points, spaced linearly in wavelengths from 450 to 1000 nm. Absorption was calculated from 1-R-T.

Simulation. Full-field, 3D simulations were performed using Lumerical FDTD, a commercial electromagnetics software package. At normal incidence, the infinite periodicity of the nanowire arrays was rendered using periodic boundary conditions and, at non-normal incidence, Bloch boundary conditions to enforce phase continuity. Symmetric boundary conditions were applied when relevant to reduce computation time. In the axial direction, perfectly matched layers were used to emulate infinite space above and below the array. All nanowire structures were modeled using Palik data for InP, Ag, Cr, and SiO_2, and ellipsometric data for PDMS.

Simulated spectra in Figure 1 used a single, broadband (450−1000 nm) simulation; for greater accuracy, simulated spectra in Figures S2 and S3 used a single wavelength, polarized infinite plane wave source, and each spectrum is composed of $276n$ simulations, spaced linearly in wavelength from 450 to 1000 nm, where n is the number of polarizations necessary to capture the unpolarized optical response of the array. Planar power monitors were used to extract the array absorption and also to distinguish between absorption in the InP and the other materials.

Image analysis of SEM images was used to determine the range of nanowire dimensions within the array; each of the arrays contained a significant distribution of nanowire geometries due in large part to the high temperature and high power InP etch. For the simulated spectra in Figure 1, simulation sweeps of the full experimental dimension range were performed, and a linear least-squares fit was used to fit the experimental absorption data. For Figures S2 and S3, a more computationally conservative approach was needed due to the computational cost of single wavelength simulations at multiple angles and polarizations. In light of this, three representative geometries were chosen for each sample; the simulated spectra in Figure 2 is a standard arithmetic mean of the three selected geometries and the simulated spectra in Figure 3 is a weighted average, in which the coefficients were determined from a linear least-squares fit to the single pass, normal incidence experimental spectra (Figure 3a, red line), similar to the spectra in Figure 1. The nanowires in Figures S1 and S3 were rendered as truncated cones and the nanowires in Figure 2 were rendered as a stack of two truncated cones to capture their complex axial profile. The remaining SiO_2 and Cr masks were modeled as truncated cones with bottom radius matching the top radius of the nanowire and a top radius of 10 nm. Precise simulated dimensions are summarized in the Supporting Information. A finer mesh was used around the nanowire, with a mesh cell width of one tenth the smallest radius.

DOI: 10.1021/acsphotonics.6b00341
ACS Photonics XXXX, XXX, XXX−XXX

■ ASSOCIATED CONTENT

Supporting Information

The Supporting Information is available free of charge on the ACS Publications website at DOI: 10.1021/acsphotonics.6b00341.

A quantitative analysis of absorption in each material contained in the InP nanowire array; tabulated values of nanowire array dimensions used in simulation (PDF).

■ AUTHOR INFORMATION

Corresponding Author

*E-mail: katherine.fountaine@ngc.com.

Notes

The authors declare no competing financial interest.

■ ACKNOWLEDGMENTS

This material is based upon work primarily supported by (C.R.B. and H.A.A.) the Engineering Research Center Program of the National Science Foundation and the Office of Energy Efficiency and Renewable Energy of the Department of Energy under NSF Cooperative Agreement No. EEC-1041895 and is also based upon work performed by (W.-H.C. and K.T.F.) the Joint Center for Artificial Photosynthesis, a DOE Energy Innovation Hub, supported through the Office of Science of the U.S. Department of Energy under Award Number DE-SC0004993.

■ REFERENCES

(1) Ra'di, Y.; Simovski, C. R.; Tretyakov, S. A. Thin Perfect Absorbers for Electromagnetic Waves: Theory, Design, and Realizations. *Phys. Rev. Appl.* **2015**, *3*, 37.

(2) Soukoulis, C. M.; Wegener, M. Past achievements and future challenges in the development of three-dimensional photonic metamaterials. *Nat. Photonics* **2011**, *5*, 523−530.

(3) Landy, N. I.; Sajuyigbe, S.; Mock, J. J.; Smith, D. R.; Padilla, W. J. Perfect metamaterial absorber. *Phys. Rev. Lett.* **2008**, *100*, 4.

(4) Sakr, E.; Dhaka, S.; Bermel, P. *Proc. SPIE* **2016**, 97431D−97431D-8.

(5) Argyropoulos, C.; Le, K. Q.; Mattiucci, N.; D'Aguanno, G.; Alu, A. Broadband absorbers and selective emitters based on plasmonic Brewster metasurfaces. *Phys. Rev. B: Condens. Matter Mater. Phys.* **2013**, *87*, 6.

(6) Liu, X. L.; Tyler, T.; Starr, T.; Starr, A. F.; Jokerst, N. M.; Padilla, W. J. Taming the Blackbody with Infrared Metamaterials as Selective Thermal Emitters. *Phys. Rev. Lett.* **2011**, *107*, 4.

(7) Khanikaev, A. B.; Wu, C. H.; Shvets, G. Fano-resonant metamaterials and their applications. *Nanophotonics* **2013**, *2*, 247−264.

(8) Liu, N.; Mesch, M.; Weiss, T.; Hentschel, M.; Giessen, H. Infrared Perfect Absorber and Its Application As Plasmonic Sensor. *Nano Lett.* **2010**, *10*, 2342−2348.

(9) Zhu, J.; Yu, Z. F.; Burkhard, G. F.; Hsu, C. M.; Connor, S. T.; Xu, Y. Q.; Wang, Q.; McGehee, M.; Fan, S. H.; Cui, Y. Optical Absorption Enhancement in Amorphous Silicon Nanowire and Nanocone Arrays. *Nano Lett.* **2009**, *9*, 279−282.

(10) Fountaine, K. T.; Kendall, C. G.; Atwater, H. A. Near-unity broadband absorption designs for semiconducting nanowire arrays via localized radial mode excitation. *Opt. Express* **2014**, *22*, A930−A940.

(11) Salisbury, W. W. Absorbent body for electromagnetic waves. Google Patents US 2599944 A, 1952.

(12) de Abajo, F. J. G. Colloquium: Light scattering by particle and hole arrays. *Rev. Mod. Phys.* **2007**, *79*, 1267−1290.

(13) Kats, M. A.; Capasso, F. Ultra-thin optical interference coatings on rough and flexible substrates. *Appl. Phys. Lett.* **2014**, *105*, 3.

(14) Laroche, M.; Albaladejo, S.; Gomez-Medina, R.; Saenz, J. J. Tuning the optical response of nanocylinder arrays: An analytical study. *Phys. Rev. B: Condens. Matter Mater. Phys.* **2006**, *74*, 5.

(15) Diedenhofen, S. L.; Grzela, G.; Haverkamp, E.; Bauhuis, G.; Schermer, J. J.; Rivas, J. G. Broadband and omnidirectional anti-reflection layer for III/V multi-junction solar cells. *Sol. Energy Mater. Sol. Cells* **2012**, *101*, 308−314.

(16) Basu, S.; Zhang, Z. M.; Fu, C. J. Review of near-field thermal radiation and its application to energy conversion. *Int. J. Energy Res.* **2009**, *33*, 1203−1232.

(17) Atwater, H.; Polman, A.; Kosten, E.; Callahan, D.; Spinelli, P.; Eisler, C.; Escarra, M.; Warmann, E.; Flowers, C., Nanophotonic design principles for ultrahigh efficiency photovoltaics. In *Nobel Symposium 153: Nanoscale Energy Converters*; Linke, H., Borgstrom, M., Pullerits, T.; Samuelson, L., Sundstrom, V., Inganas, O., Eds.; Amer Inst Physics: Melville, 2013; Vol. *1519*, pp 17−21.

(18) Callahan, D. M.; Munday, J. N.; Atwater, H. A. Solar Cell Light Trapping beyond the Ray Optic Limit. *Nano Lett.* **2012**, *12*, 214−218.

(19) de Abajo, F. J. G. Graphene Plasmonics: Challenges and Opportunities. *ACS Photonics* **2014**, *1*, 135−152.

(20) Brar, V. W.; Jang, M. S.; Sherrott, M.; Lopez, J. J.; Atwater, H. A. Highly Confined Tunable Mid-Infrared Plasmonics in Graphene Nanoresonators. *Nano Lett.* **2013**, *13*, 2541−2547.

(21) Kats, M. A.; Sharma, D.; Lin, J.; Genevet, P.; Blanchard, R.; Yang, Z.; Qazilbash, M. M.; Basov, D. N.; Ramanathan, S.; Capasso, F. Ultra-thin perfect absorber employing a tunable phase change material. *Appl. Phys. Lett.* **2012**, *101*, 5.

(22) Liu, X. L.; Starr, T.; Starr, A. F.; Padilla, W. J. Infrared Spatial and Frequency Selective Metamaterial with Near-Unity Absorbance. *Phys. Rev. Lett.* **2010**, *104*, 4.

(23) Chou, J. B.; Yeng, Y. X.; Lenert, A.; Rinnerbauer, V.; Celanovic, I.; Soljacic, M.; Wang, E. N.; Kim, S. G. Design of wide-angle selective absorbers/emitters with dielectric filled metallic photonic crystals for energy applications. *Opt. Express* **2014**, *22*, A144−A154.

(24) Gudiksen, M. S.; Lauhon, L. J.; Wang, J.; Smith, D. C.; Lieber, C. M. Growth of nanowire superlattice structures for nanoscale photonics and electronics. *Nature* **2002**, *415*, 617−620.

(25) Park, H.; Dan, Y.; Seo, K.; Yu, Y. J.; Duane, P. K.; Wober, M.; Crozier, K. B. Filter-Free Image Sensor Pixels Comprising Silicon Nanowires with Selective Color Absorption. *Nano Lett.* **2014**, *14*, 1804−1809.

(26) Soci, C.; Zhang, A.; Bao, X. Y.; Kim, H.; Lo, Y.; Wang, D. L. Nanowire Photodetectors. *J. Nanosci. Nanotechnol.* **2010**, *10*, 1430−1449.

(27) Liu, X. L.; Wang, L. P.; Zhang, Z. M. Wideband Tunable Omnidirectional Infrared Absorbers Based on Doped-Silicon Nanowire Arrays. *J. Heat Transfer* **2013**, *135*, 8.

(28) Tilke, A. T.; Pescini, L.; Lorenz, H.; Blick, R. H. Fabrication and transport characterization of a primary thermometer formed by Coulomb islands in a suspended silicon nanowire. *Appl. Phys. Lett.* **2003**, *82*, 3773−3775.

(29) Anttu, N.; Xu, H. Q. Coupling of Light into Nanowire Arrays and Subsequent Absorption. *J. Nanosci. Nanotechnol.* **2010**, *10*, 7183−7187.

(30) Garnett, E.; Yang, P. D. Light Trapping in Silicon Nanowire Solar Cells. *Nano Lett.* **2010**, *10*, 1082−1087.

(31) Cao, L.; Fan, P.; Vasudev, A. P.; White, J. S.; Yu, Z.; Cai, W.; Schuller, J. A.; Fan, S.; Brongersma, M. L. Semiconductor nanowire optical antenna solar absorbers. *Nano Lett.* **2010**, *10*, 439−445.

(32) Hu, S.; Chi, C. Y.; Fountaine, K. T.; Yao, M. Q.; Atwater, H. A.; Dapkus, P. D.; Lewis, N. S.; Zhou, C. W. Optical, electrical, and solar energy-conversion properties of gallium arsenide nanowire-array photoanodes. *Energy Environ. Sci.* **2013**, *6*, 1879−1890.

(33) Liu, C.; Tang, J. Y.; Chen, H. M.; Liu, B.; Yang, P. D.; Fully, A. Integrated Nanosystem of Semiconductor Nanowires for Direct Solar Water Splitting. *Nano Lett.* **2013**, *13*, 2989−2992.

(34) Woodhouse, M.; Goodrich, A. *Manufacturing Cost Analysis Relevant to Single-and Dual-Junction Photovoltaic Cells Fabricated with*

DOI: 10.1021/acsphotonics.6b00341
ACS Photonics XXXX, XXX, XXX−XXX

III-Vs and III-Vs Grown on Czochralski Silicon (Presentation); National Renewable Energy Laboratory (NREL), Golden, CO, 2014.
(35) Rosenwaks, Y.; Shapira, Y.; Huppert, D. Evidence for Low Intrinsic Surface-Recombination Velocity on p-Type InP. *Phys. Rev. B: Condens. Matter Mater. Phys.* **1991**, *44*, 13097−13100.
(36) Grzela, G.; Paniagua-Domínguez, R.; Barten, T.; Fontana, Y.; Sánchez-Gil, J. A.; Gómez Rivas, J. Nanowire antenna emission. *Nano Lett.* **2012**, *12*, 5481−5486.
(37) Muskens, O. L.; Rivas, J. G.; Algra, R. E.; Bakkers, E.; Lagendijk, A. Design of light scattering in nanowire materials for photovoltaic applications. *Nano Lett.* **2008**, *8*, 2638−2642.
(38) Fan, Z. Y.; Kapadia, R.; Leu, P. W.; Zhang, X. B.; Chueh, Y. L.; Takei, K.; Yu, K.; Jamshidi, A.; Rathore, A. A.; Ruebusch, D. J.; Wu, M.; Javey, A. Ordered Arrays of Dual-Diameter Nanopillars for Maximized Optical Absorption. *Nano Lett.* **2010**, *10*, 3823−3827.
(39) Lin, C. X.; Povinelli, M. L. Optical absorption enhancement in silicon nanowire arrays with a large lattice constant for photovoltaic applications. *Opt. Express* **2009**, *17*, 19371−19381.
(40) Abujetas, D. R.; Paniagua-Dominguez, R.; Sanchez-Gil, J. A. Unraveling the Janus Role of Mie Resonances and Leaky/Guided Modes in Semiconductor Nanowire Absorption for Enhanced Light Harvesting. *ACS Photonics* **2015**, *2*, 921−929.
(41) Seo, K.; Wober, M.; Steinvurzel, P.; Schonbrun, E.; Dan, Y. P.; Ellenbogen, T.; Crozier, K. B. Multicolored Vertical Silicon Nanowires. *Nano Lett.* **2011**, *11*, 1851−1856.
(42) Heiss, M.; Russo-Averchi, E.; Dalmau-Mallorqui, A.; Tutuncuoglu, G.; Matteini, F.; Ruffer, D.; Conesa-Boj, S.; Demichel, O.; Alarcon-Llado, E.; Morral, A. F. I. III−V nanowire arrays: growth and light interaction. *Nanotechnology* **2014**, *25*, 9.
(43) Wallentin, J.; Anttu, N.; Asoli, D.; Huffman, M.; Aberg, I.; Magnusson, M. H.; Siefer, G.; Fuss-Kailuweit, P.; Dimroth, F.; Witzigmann, B.; Xu, H. Q.; Samuelson, L.; Deppert, K.; Borgstrom, M. T. InP Nanowire Array Solar Cells Achieving 13.8% Efficiency by Exceeding the Ray Optics Limit. *Science* **2013**, *339*, 1057−1060.
(44) Diedenhofen, S. L.; Janssen, O. T. A.; Grzela, G.; Bakkers, E.; Rivas, J. G. Strong Geometrical Dependence of the Absorption of Light in Arrays of Semiconductor Nanowires. *ACS Nano* **2011**, *5*, 2316−2323.
(45) Deinega, A.; John, S. Solar power conversion efficiency in modulated silicon nanowire photonic crystals. *J. Appl. Phys.* **2012**, *112*, 7.
(46) Hong, L.; Rusli; Wang, X. C.; Zheng, H. Y.; Wang, H.; Yu, H. Y. Design guidelines for slanting silicon nanowire arrays for solar cell application. *J. Appl. Phys.* **2013**, *114*, 6.
(47) Cansizoglu, H.; Cansizoglu, M. F.; Finckenor, M.; Karabacak, T. Optical Absorption Properties of Semiconducting Nanostructures with Different Shapes. *Adv. Opt. Mater.* **2013**, *1*, 158−166.
(48) Lin, C. X.; Huang, N. F.; Povinelli, M. L. Effect of aperiodicity on the broadband reflection of silicon nanorod structures for photovoltaics. *Opt. Express* **2012**, *20*, A125−A132.
(49) Vynck, K.; Burresi, M.; Riboli, F.; Wiersma, D. S. Photon management in two-dimensional disordered media. *Nat. Mater.* **2012**, *11*, 1017−1022.
(50) Snyder, A. W.; Love, J. *Optical Waveguide Theory*; Springer, 1983.
(51) Kelzenberg, M. *Silicon Microwire Photovoltaics*; California Institute of Technology, 2010.

DOI: 10.1021/acsphotonics.6b00341
ACS Photonics XXXX, XXX, XXX−XXX